ACS OMEGA

Open Access

http://pubs.acs.org/journal/acsodf

Article

Synthesis and Characterization of Zeolite A from Industrial Fly Ash as a Green, Cost-Effective Cd^{2+} and Pb^{2+} Adsorbent for Wastewater Applications

Darunee Sukchit, Malee Prajuabsuk, Saisamorn Lumlong, Chan Inntam, Auradee Punkvang, Sasijuta Wattanarach, Parjaree Thavorniti, Bunjerd Jongsomjit, Kanitta Wongyai, Duangkamol Gleeson, Paramasivam Shanmugam, Supakorn Boonyuen, and Pornpan Pungpo*

Cite This: *ACS Omega* 2025, 10, 5981−5992

Read Online

ACCESS | Metrics & More | Article Recommendations | Supporting Information

ABSTRACT: According to the large amount of fly ash waste generated from the use of lignite coal as the primary fuel for electricity generation in the Mae Moh district of Lampang province, Thailand, efforts have been made in waste management to reduce and repurpose this industrial byproduct. In this study, lignite coal fly ash was used to synthesize zeolite A adsorbents for the treatment of wastewater contaminated with heavy metals. Characterization of the synthesized zeolite using XRD, XRF, BET, and SEM methods confirmed that it is zeolite A, with a calculated Si/Al molar ratio of approximately 1.19, closely matching the theoretical ratio of zeolite A. This zeolite A exhibited a high crystalline phase and a mesoporous structure, having a specific surface area of 37.10 m^2/g and a total pore volume of 0.06 cm^3/g. The performance of this zeolite A was evaluated for the adsorption of Cd^{2+} and Pb^{2+} in prepared solutions. The removal efficiencies of zeolite A for Cd^{2+} and Pb^{2+} were 99.65% ± 0.1% and 93.90% ± 0.5%, with maximum adsorption capacities of 17.3 ± 0.6 and 8.8 ± 0.1 mg/g, respectively. Additionally, zeolite A demonstrated reusability for the adsorption of Cd^{2+} and Pb^{2+}, maintaining a removal efficiency of 80.52% ± 0.1% for Cd^{2+} over five reuse cycles, and 96.83% ± 0.7% for Pb^{2+} over one reuse cycle. The adsorption of Cd^{2+} and Pb^{2+} by zeolite A followed the Langmuir isotherm model and pseudo-second-order kinetic model. Moreover, the adsorption of Cd^{2+} and Pb^{2+} by zeolite A was found to be a spontaneous, endothermic process, as evidenced by increasingly negative Gibbs free energy change ($\Delta G°$) values with rising temperature. Density functional theory (DFT) calculations were also performed to investigate the binding of Cd^{2+} and Pb^{2+} ions to zeolite A, providing insight into why Cd^{2+} exhibits a slightly higher affinity than Pb^{2+}. The results showed that Cd^{2+} ions have a marginally greater affinity for zeolite A compared to Pb^{2+} (−85.72 vs −85.39 kcal/mol), which aligns with experimental findings. This study offers an alternative approach for reducing industrial waste by repurposing it for valuable applications, contributing to sustainable waste management practices that align with the principles of the bio-circular-green economy.

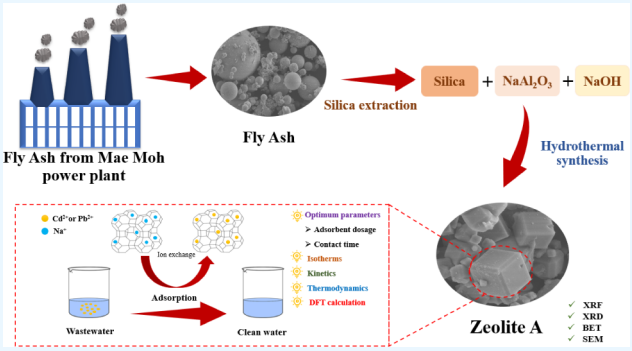

1. INTRODUCTION

Lignite coal fly ash contains 35−60% silica (SiO_2), 10−30% alumina (Al_2O_3), 4−20% ferric oxide (Fe_2O_3), and 1−35% calcium oxide (CaO),[1] and is classified into two broad classes, C and F.[2] As a result, this fly ash has been used as an additive in construction materials, a soil-texturing amendment in agriculture, and as an adsorbent.[3,4] Furthermore, fly ash has served as a source of silica and alumina for the synthesis of zeolites,[5,6] a porous material used in adsorbents, catalysts, membranes, biomedical, and agricultural applications.[7−12] Zeolites, with their high surface area, excellent cation-exchange efficiency, and low manufacturing costs,[13] are highly effective adsorbents for removing toxic heavy metal ions from contaminated wastewater,[14] making them valuable for wastewater treatment.[15,16] Zeolite A ($Na_{12}[AlO_2SiO_2]_{12}·27H_2O$), which has a three-dimensional cubic crystalline structure with an equivalent ratio of silica to alumina,[16,17] is one of the most significant types of zeolite used for environmental applications, particularly for the removal of toxic heavy metals.[18−21]

Toxic heavy metal ions, such as Cd^{2+}, Pb^{2+}, Ni^{2+}, Cu^{2+}, Zn^{2+}, and others,[22] released into the environment mainly from

Received: November 2, 2024
Revised: January 14, 2025
Accepted: January 22, 2025
Published: February 4, 2025

Table 1. Chemical Composition of Fly Ash, Extracted SiO_2, and Zeolite A (% by Weight)

Component	SiO_2	Al_2O_3	CaO	Fe_2O_3	SO_3	Na_2O	K_2O	MgO	Others
fly ash	35.60	18.60	19.00	12.40	6.61	1.96	2.30	2.24	1.29
extracted SiO_2	95.20	1.24	0.05	0.17	0.02	1.62	0.13	0.18	1.39
zeolite A	45.70	38.30	0.33	0.05	0.01	15.30	0.07	0.14	0.10

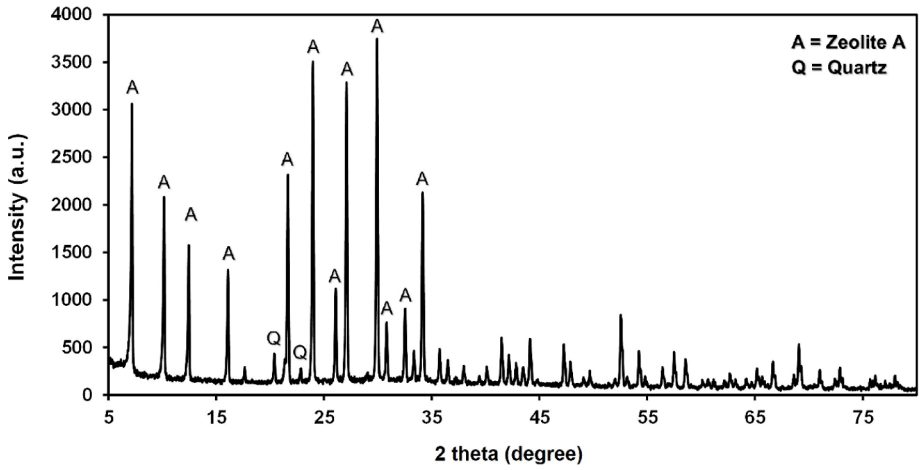

Figure 1. X-ray diffraction patterns of zeolite A.

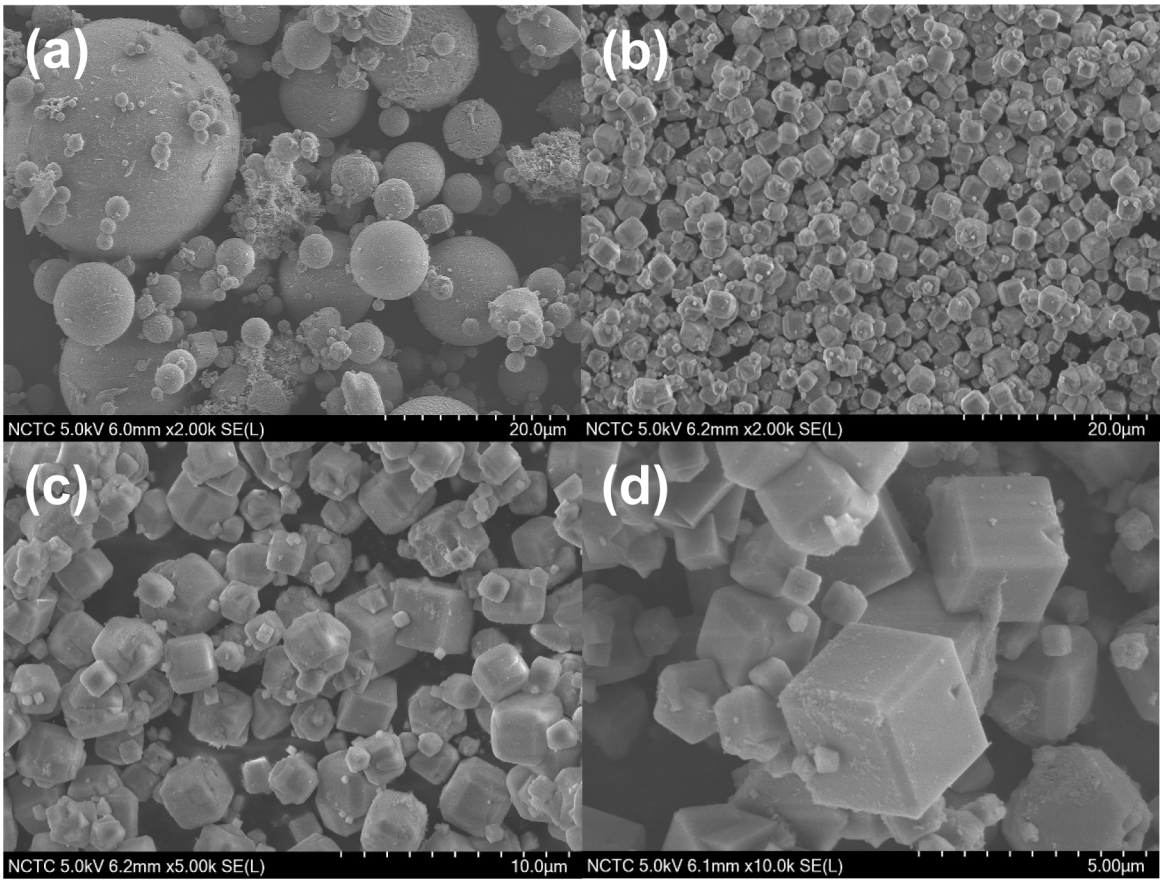

Figure 2. SEM images of fly ash (a) and synthesized zeolite A (b–d) at different magnification levels.

industrial waste,[23,24] have become serious problems for human health due to these toxic metals entering the food chain.[25] Various methods have been used for the removal of these heavy metal ions, including membrane filtration,[26−29] chemical precipitation,[30,31] electrolytic removal,[32] ion exchange,[33,34] and adsorption.[35] The adsorption method is widely used for metal ion removal due to its ability to remove trace amounts, high efficiency, cost-effectiveness, easy operation, and broad adaptability.[36−38]

https://doi.org/10.1021/acsomega.4c09990
ACS Omega 2025, 10, 5981−5992

The power plant in Mae Moh district, Lampang province, Thailand, uses lignite coal as its main fuel, which produces large quantities of fly ash waste as a byproduct, approximately 6000 tons per day. In our present work, this lignite coal fly ash was utilized as a low-cost material for the synthesis of zeolite A. Additionally, the effectiveness of zeolite A was evaluated for the adsorption of Cd^{2+} and Pb^{2+} from prepared solutions, with the aim of using it for the treatment of wastewater contaminated with toxic metal ions in the future.

2. RESULTS AND DISCUSSION

2.1. Characterizations of Samples. *2.1.1. X-ray Fluorescence (XRF) Spectrum Analysis of the Raw Material and Zeolite A.* The fly ash in this study was obtained from the Mae Moh power plant, Lampang. The chemical compositions of fly ash were characterized by the XRF method. Table 1 lists the chemical compositions of fly ash. The fly ash from the power plant contains 35.60% by weight of SiO_2 and 18.60% by weight of Al_2O_3, which accounted for 54.20% of the total mass of fly ash. In addition, it included 19.00% by weight of CaO, 12.40% by weight of Fe_2O_3, and 6.61% by weight of SO_3. The combination of SiO_2, Al_2O_3, and Fe_2O_3 was 66.60% by weight, which was classified as class C, in accordance with the ASTM C318 standard.[50] The Si/Al ratio of 1.91 calculated for the fly ash indicates that it is suitable for synthesizing aluminum-rich zeolites, such as zeolite A (Si/Al = 1−1.25).[51−53] To remove the impurities and increase the purity of silica from fly ash, the extract was pretreated by the alkaline leaching method. The composition of silica (SiO_2) was obtained with 95.20% by weight, while other compositions in fly ash were decreased as shown in Table 1. These results were described by the reactions of metal oxides with acid. The synthesis of zeolite A by alkali melting and the hydrothermal method contains 45.70% by weight of SiO_2, 38.30% by weight of Al_2O_3, and 15.30% by weight of Na_2O, in which the calculated molar ratio of Si/Al of the product is around 1.19, which is close to the theoretical molar ratio of zeolite A.

2.1.2. X-ray Diffraction (XRD) Analysis. In order to confirm that the synthesized zeolite in this work is zeolite A, the XRD pattern of the synthesized sample is elucidated. The experimental results showed that the synthesis of zeolite A by the hydrothermal method is achieved. The intensities of the major XRD peaks at 2θ values of 12.5°, 16.1°, 21.7°, 30°, and 34.2° were considered. The characteristic diffraction peaks observed are generally consistent with the standard diffraction peaks of zeolite A (PDF#39−0222). This indicates the presence of the zeolite A structure. The characteristic peaks of the synthesized zeolite A are located at 7.2°, 10.1°, 12.4°, 16.2°, 21.6°, 24°, 26°, 27°, 30°, 30.8°, 32.5°, and 34°, as shown in Figure 1. This confirmed that this synthetic zeolite is zeolite A, and this XRD pattern showed a high crystalline phase.

2.1.3. Scanning Electron Microscope (SEM) Analysis. SEM characterization was employed to examine the textural properties of fly ash and synthesized zeolite A. The morphologies of fly ash and synthesized zeolite A are shown in Figure 2. The fly ash particles mainly exhibit a spherical morphology (cenospheres) with a smooth surface as presented in Figure 2a, which originates from the Si and Al, plus some impurities such as Fe and Ca.[54] This was confirmed by the XRF analysis of fly ash, which presented high compositions of CaO and Fe_2O_3 as seen in Table 1. In addition, the morphology of synthesized zeolite A revealed the formation of cubic crystals with rough and smooth surfaces. This is characteristic of zeolite A (LTA framework topology). This occurs because the zeolitic complex lattice has a negative charge generated by the difference between $[AlO_4]^-$ and $[SiO_4]^-$ tetrahedra in the hydrothermal process between both of them.

2.1.4. BET Surface Area and Thermal Gravimetric (TG) Analysis. N_2 physisorption analysis was applied to determine the surface area of zeolite A before and after adsorbing toxic metals. The specific surface areas of zeolite A before and after adsorbing toxic metals were determined using the BET equation, while the pore size and pore volume were estimated using the Barrett−Joyner−Halenda (BJH) method, as shown in Table 2. The N_2 adsorption−desorption isotherms of zeolite A before and after adsorbing toxic metals, as shown in Figure 3, were evaluated to assess the preferable surface areas of the adsorbents. This zeolite A exhibits an obvious hysteresis loop at relative pressures of P/P_0 > 0.5, which is characteristic of a type IV isotherm, indicating a typical mesoporous structure. The aperture distribution curve reveals that zeolite A has a continuous pore distribution ranging from 2 to 50 nm. Furthermore, Figure 3 shows the BET images before and after the adsorption of Cd^{2+} and Pb^{2+} on the zeolite. The obtained results indicate that, after adsorption, the specific surface area is drastically reduced. The specific surface area and total pore volume of the synthesized zeolite A were 37.10 m^2/g and 0.06 cm^3/g, respectively. After the adsorption of toxic metals, these values changed to 2.84 m^2/g for the specific surface area and 0.02 cm^3/g for the total pore volume, as shown in Table 2.[55] These results reveal that the toxic metals are adsorbed onto the surface of zeolite A. Furthermore, the thermal stability of the prepared zeolite A was characterized by TGA analysis, as shown in Figure S3.

Table 2. Surface Area and Pore Volume of the Zeolite A Adsorbents

Adsorbent	BET surface area (m^2/g)	Total pore volume (cm^3/g)
before adsorption	37.10	0.06
after adsorption	2.84	0.02

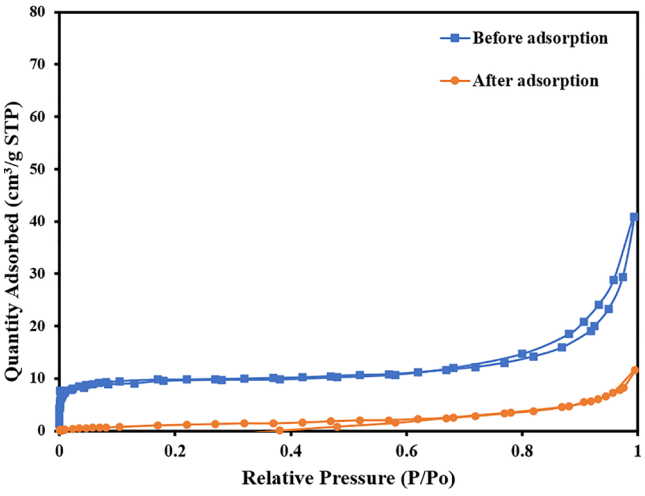

Figure 3. N_2 adsorption−desorption isotherm.

2.2. The Adsorbent Dosage for Cd^{2+} and Pb^{2+} Adsorption. Different dosages of zeolite A were used to investigate its effect on the adsorption behavior of Cd^{2+} and Pb^{2+}. Zeolite A dosages were varied from 1 to 10 g/L for Cd^{2+} adsorption and from 1 to 8 g/L for Pb^{2+} adsorption. The

https://doi.org/10.1021/acsomega.4c09990
ACS Omega 2025, 10, 5981−5992

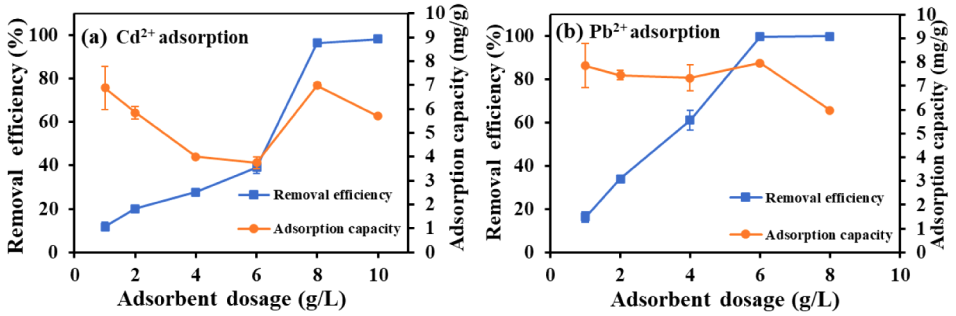

Figure 4. Effect of adsorbent dosage on the adsorption of Cd^{2+} (a) and Pb^{2+} (b) by zeolite A. Initial concentration of Cd^{2+} and Pb^{2+}: 50 mg/L; adsorbent dosage: 1, 2, 4, 6, 8, and 10 g/L for Cd^{2+} and 1, 2, 4, 6, and 8 g/L for Pb^{2+}; the contact time: 60 min; pH = 6; T = 25 °C; V = 25 mL.

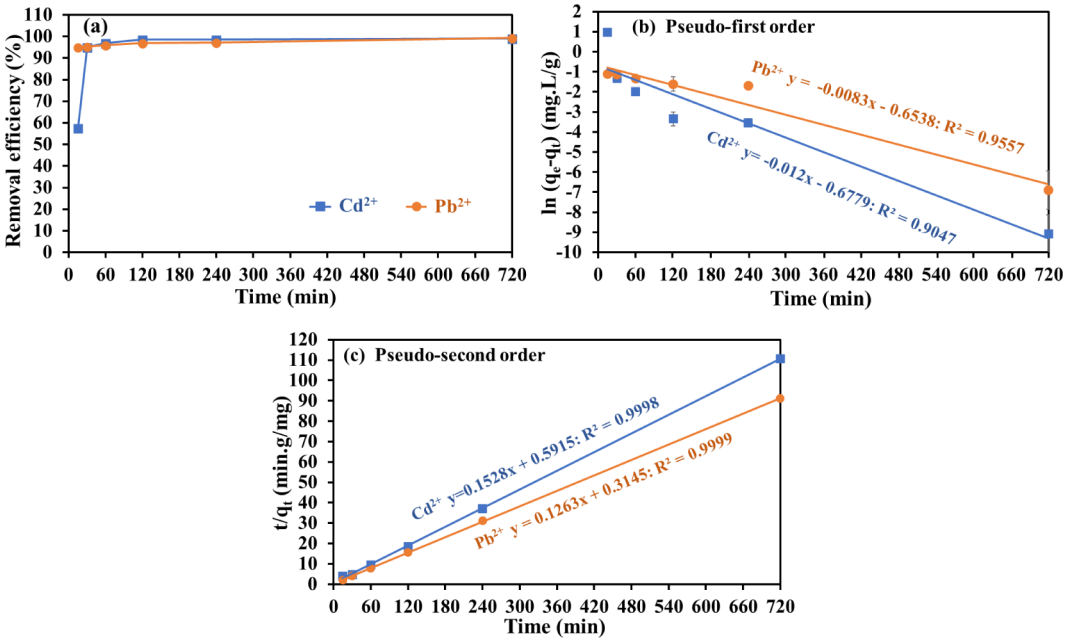

Figure 5. Contact time of Cd^{2+} and Pb^{2+} on adsorption by zeolite A and the adsorption kinetic models of zeolite A. Removal efficiency for Cd^{2+} and Pb^{2+} (a), the pseudo-first-order model (b), and the pseudo-second-order model (c). Contact times for Cd^{2+} and Pb^{2+}: 15, 30, 60, 120, 240, and 720 min; adsorbent dosages: 8 g/L for Cd^{2+} and 6 g/L for Pb^{2+}; initial concentrations of Cd^{2+} and Pb^{2+}: 50 mg/L; pH = 6; T = 25 °C; V = 25 mL.

removal efficiency and capacity of zeolite A for removing Cd^{2+} and Pb^{2+} from aqueous solutions were determined, as illustrated in Figure 4. The increase in zeolite A dosage from 1 to 10 g/L resulted in a nearly 100% improvement in Cd^{2+} removal efficiency. However, the difference in removal efficiency between 8 and 10 g/L of zeolite A was minimal, with values of 96.44% ± 1.3% and 98.25% ± 0.1%, respectively (Figure 4a). Notably, the adsorption capacity at 8 g/L (6.99 mg/g) was higher than that at 10 g/L (5.75 mg/g), indicating that the 10 g/L dosage exceeded the optimal amount for Cd^{2+} adsorption. Consequently, a dosage of 8 g/L was chosen for further Cd^{2+} adsorption investigation. A similar trend was observed for Pb^{2+} adsorption. However, the optimal dosage of zeolite A for Pb^{2+} adsorption was found to be 6 g/L, which provided both a high removal efficiency and a high adsorption capacity (Figure 4b). Therefore, this dosage was selected for further investigation of Pb^{2+} adsorption.

2.3. Adsorption Kinetics for Cd^{2+} and Pb^{2+}. The optimal dosages of zeolite A, identified as 8 g/L for Cd^{2+} and 6 g/L for Pb^{2+} adsorption, were used to evaluate the effect of contact time on the adsorption of Cd^{2+} and Pb^{2+}. Adsorption was tested at intervals of 15, 30, 60, 120, 240, and 720 min. The removal efficiency for Cd^{2+} increased sharply from 57.33% ± 1.5% to 95.02% ± 0.8% as the contact time increased from 15 to 30 min. After this, the removal efficiency showed a gradual increase to 96.98% ± 0.5%, 98.54% ± 0.1%, 98.63% ± 0.3%, and 99.06% ± 0.1% at 60, 120, 240, and 720 min, respectively (Figure 5a). These results indicate that the adsorption of Cd^{2+} reached equilibrium at approximately 30 min. In contrast, the adsorption of Pb^{2+} reached equilibrium more quickly, as shown by the removal efficiencies at 15, 30, 60, 120, 240, and 720 min, which increased slightly from 95.14% ± 0.6%, 95.21% ± 0.7%, 96.12% ± 0.6%, 96.89% ± 0.9%, 97.1% ± 0.4%, to 99.41% ± 0.1%, respectively (Figure 5a). Therefore, contact times of 30 and 15 min were selected for further investigation of the adsorption isotherms for Cd^{2+} and Pb^{2+}.

The kinetic model can explain the rate of adsorption of Cd^{2+} and Pb^{2+} by zeolite A, reflecting the equilibrium state reached and the involved adsorption mechanisms. Consequently, the kinetic models of these adsorption processes were investigated using linear plots of the pseudo-first-order model ($\ln(q_e - q_t)$ versus time) and the pseudo-second-order model (t/q_t versus time), as described by eqs 3 and 4, respectively. The correlation coefficients (R^2) obtained from the pseudo-second-order plots

https://doi.org/10.1021/acsomega.4c09990
ACS Omega 2025, 10, 5981−5992

Table 3. Parameters of Pseudo-First-Order and Pseudo-Second-Order Models

		Pseudo-first-order model			Pseudo-second-order model		
	$q_{e\text{-}exp}$ (mg/g)	$q_{e\text{-}cal}$ (mg/g)	k_1 (min^{-1})	R^2	$q_{e\text{-}cal}$ (mg/g)	k_2 (g/mg.min)	R^2
Cd^{2+}	6.50	1.97	0.012	0.90	6.54	0.04	0.99
Pb^{2+}	7.90	1.92	0.008	0.96	7.92	0.05	0.99

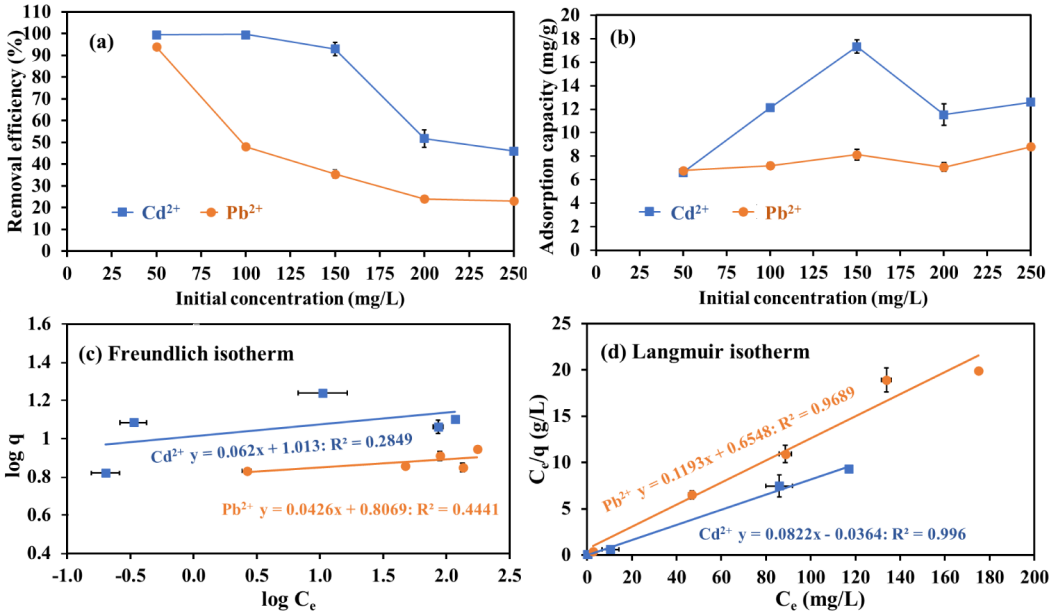

Figure 6. Effect of initial Cd^{2+} and Pb^{2+} concentrations on the adsorption by zeolite A and the adsorption isotherm models of zeolite A. Removal efficiency and adsorption capacity for Cd^{2+} (a) and Pb^{2+} (b); Freundlich isotherm (c) and Langmuir isotherm (d). Initial concentrations of Cd^{2+} and Pb^{2+}: 50, 100, 150, 200, and 250 mg/L; adsorbent dosages: 8 g/L for Cd^{2+} and 6 g/L for Pb^{2+}; contact times: 30 min for Cd^{2+} and 15 min for Pb^{2+}; pH = 6; T = 25 °C; V = 25 mL.

Table 4. Adsorption Isotherm Parameters of Cd^{2+} and Pb^{2+} onto Zeolite A

	Langmuir isotherm			Freundlich isotherm			
Adsorbate	q_{max} (mg/g)	R_L	R^2	$1/n$	n	K_F	R^2
Cd^{2+}	12.2	0.002−0.008	0.996	0.06	16.13	10.30	0.285
Pb^{2+}	8.4	0.02−0.1	0.969	0.04	23.47	6.41	0.444

for Cd^{2+} and Pb^{2+} (Figure 5c) are higher than those from the pseudo-first-order plots (Figure 5b). Therefore, the adsorption of both ions by zeolite A follows the pseudo-second-order model, with R^2 values of 0.9998 and 0.9999, respectively. Moreover, the equilibrium adsorption capacities calculated from the pseudo-second-order model ($q_{e\text{-}cal}$) for Cd^{2+} and Pb^{2+} are 6.54 and 7.92 mg/g, respectively, which are consistent with the experimental values ($q_{e\text{-}exp}$) of 6.50 and 7.90 mg/g (Table 3). These results indicate that the pseudo-second-order model is able to predict the experimental adsorption capacities of Cd^{2+} and Pb^{2+} on zeolite A.

2.4. Adsorption Isotherm for Cd^{2+} and Pb^{2+}. The removal efficiency and adsorption capacity of zeolite A were determined by varying the initial concentrations of Cd^{2+} and Pb^{2+} at 50, 100, 150, 200, and 250 mg/L. Initial concentrations of Cd^{2+} above 100 mg/L and Pb^{2+} above 50 mg/L decreased the removal efficiency from 99.65% ± 0.1% to 46.00% ± 0.3% and from 93.90% ± 0.5% to 23.17% ± 0.2%, respectively (Figure 6a), indicating an excess of Cd^{2+} and Pb^{2+} saturating the available adsorption sites of zeolite A. The maximum adsorption capacity of zeolite A for Cd^{2+} and Pb^{2+} was 17.3 ± 0.6 and 8.8 ± 0.1 mg/g, respectively (Figure 6b). The removal efficiencies of Cd^{2+} and Pb^{2+} reported in our study are comparable to previously reported values of 96.9% and 100% for synthetic zeolite NaA prepared from lithium leach residue.[56] Subsequently, the adsorption capacities of zeolite A, obtained from the differences in initial concentration, were used to investigate the adsorption isotherms of zeolite A.

The adsorption isotherms of Cd^{2+} and Pb^{2+} onto zeolite A were determined using linear plots of the Langmuir (C_e/q versus C_e) and Freundlich ($\log q$ versus $\log C_e$) models, as described by eqs 5 and 7, respectively. The R^2 values of 0.285 and 0.444 for the Freundlich model, observed for both Cd^{2+} and Pb^{2+} adsorption (Figure 6c), indicate a weak correlation between $\log q$ and $\log C_e$, suggesting that this model does not adequately describe the adsorption process for these ions. In contrast, the R^2 values for the Langmuir model are notably high, with 0.996 for Cd^{2+} and 0.969 for Pb^{2+} adsorption (Figure 6d), indicating the best fit. Therefore, the adsorption of Cd^{2+} and Pb^{2+} onto zeolite A follows the Langmuir isotherm, implying monolayer adsorption on a homogeneous surface, similar to what has been observed in other natural[57−59] and synthetic zeolites.[56,60] Moreover, the adsorption processes of Cd^{2+} and Pb^{2+} are favorable, as evidenced by R_L values ranging from 0.002 to 0.008 for Cd^{2+} and 0.02 to 0.1 for Pb^{2+} (Table 4). The maximum adsorption capacities (q_{max}) calculated from the Langmuir

https://doi.org/10.1021/acsomega.4c09990
ACS Omega 2025, 10, 5981−5992

model for the adsorption of Cd^{2+} and Pb^{2+} by zeolite A are 12.2 and 8.4 mg/g, respectively (Table 4), which are comparable to the experimental values of 17.3 ± 0.6 and 8.8 ± 0.1 mg/g, respectively.

2.5. Thermodynamics for Cd^{2+} and Pb^{2+} Adsorption. The thermodynamic parameters for the adsorption of Cd^{2+} and Pb^{2+} on zeolite A, including $\Delta H°$ and $\Delta S°$, obtained from the linear plots of ln K_d versus $1/T$ (Figure 7), as expressed in eq 10,

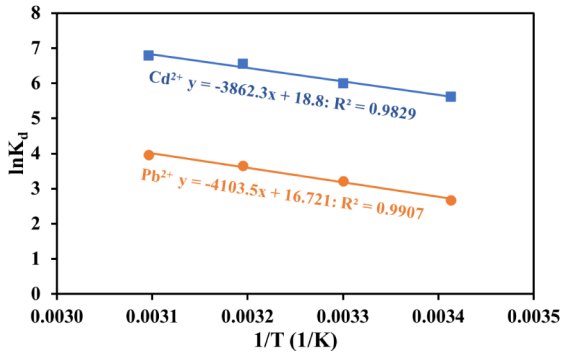

Figure 7. Plots of ln K_d versus $1/T$ for the adsorption of Cd^{2+} and Pb^{2+} on zeolite A at temperatures of 293, 303, 313, and 323 K. Initial concentrations of Cd^{2+} and Pb^{2+} were 50 mg/L; adsorbent dosages were 8 g/L for Cd^{2+} and 6 g/L for Pb^{2+}; adsorption times were 30 min for Cd^{2+} and 15 min for Pb^{2+}; pH = 6 and V = 25 mL.

are presented in Table 5. Negative values of $\Delta G°$, calculated from $\Delta H°$ and $\Delta S°$ at temperatures of 293, 303, 313, and 323 K, were observed for the adsorption of Cd^{2+} and Pb^{2+} on zeolite A (Table 5), indicating that the adsorption process is spontaneous. Moreover, more negative values of $\Delta G°$ with increasing temperature were observed for the adsorption of Cd^{2+} and Pb^{2+}, suggesting that the process is more favorable at higher temperatures. These findings are consistent with the positive values of $\Delta H°$, confirming that the process is endothermic (Table 5). The positive values of $\Delta S°$ observed for the adsorption of Cd^{2+} and Pb^{2+} indicate an increase in the disorder during the adsorption process.

2.6. Adsorption Mechanism. In this study, the adsorption of Cd^{2+} and Pb^{2+} ions on zeolite A was observed to follow the Langmuir adsorption model and the pseudo-second-order kinetic model. This indicates that the adsorption process occurs as a monolayer on the zeolite A surface,[43] with the rate-limiting step being chemisorption involving sharing or exchange of electrons between sorbent and sorbate.[42] Zeolite A features a three-dimensional framework composed of SiO_4 and AlO_4 tetrahedra, which creates a negatively charged structure. This negative charge is balanced by exchangeable positive ions, such as Na^+, K^+, and Ca^{2+}, located within the framework (Figure 8).[61,62] Therefore, we propose that the adsorption of Cd^{2+} and Pb^{2+} on zeolite A involves an ion exchange mechanism, as reported in previous studies.[62,63] When zeolite A is exposed to a solution containing Cd^{2+} or Pb^{2+} ions, these ions replace the original positive ions in the zeolite framework due to the electrostatic attraction between the positively charged metal ions and the negatively charged framework of zeolite A. Cd^{2+} and Pb^{2+} interact with the negatively charged oxygen (O^-) in the zeolite framework. The electrostatic interactions between zeolite A and these metal ions would play a critical role in this step. Subsequently, the negatively charged oxygen atoms in zeolite A, acting as excellent electron donors, donate their lone pairs to form coordinate covalent bonds with Cd^{2+} and Pb^{2+}, which act as electron acceptors by accommodating electrons in their empty orbitals (Figure 8). This chemisorption step is likely the rate-limiting stage of the adsorption process, consistent with the pseudo-second-order kinetic model. Further, the formation of the coordinate covalent bonds between Cd^{2+} or Pb^{2+} and zeolite A is supported by $\Delta G°$ values lower than −40 kcal/mol (167.36 kJ/mol) as shown in Table 5, indicating a spontaneous and strong interaction. Previous studies have reported adsorption processes with free energy values between −15 and −30 kJ/mol, suggesting the involvement of both ionic and covalent chemical reactions.[64] The adsorption of Cd^{2+} and Pb^{2+} does not significantly alter the surface functional groups of zeolite A, as revealed by FTIR and XRD characterizations (Figures S1 and S2). These results demonstrate the high stability of as-prepared zeolite A, with its crystal structure remaining intact throughout the adsorption process.

2.7. Reusability of Zeolite A for the Adsorption of Cd^{2+} and Pb^{2+}. The reusability of zeolite A for the adsorption of Cd^{2+} and Pb^{2+} was evaluated for both environmental and economic reasons. The removal efficiency of Cd^{2+} and Pb^{2+} by zeolite A after each reuse cycle is shown in Figure 9. The removal efficiency of Cd^{2+} decreased from 95.23% ± 0.6% in the first reuse cycle to 85.07% ± 0.1% in the second cycle. However, the efficiencies for the third, fourth, and fifth cycles, 83.71% ± 0.8%, 83.35% ± 0.1%, and 80.52% ± 0.1%, respectively, are comparable to that of the second cycle (85.07% ± 0.1%), indicating good reusability of zeolite A for Cd^{2+} adsorption (Figure 9a). In contrast, the removal efficiency of Pb^{2+} dramatically decreased from 96.83% ± 0.7% in the first cycle to 34.52% ± 4.1% in the second cycle, and 24.03% ± 0.6% in the third cycle, indicating the low reusability of zeolite A for Pb^{2+} adsorption (Figure 9b).

2.8. Computational Analysis on the Adsorption Energy. Metal binding to zeolite and other surfaces has been extensively used in the literature to understand binding phenomena. For example, Boekfa et al. studied the binding of palladium ions to the Lewis base sites of a 34T in their research on Suzuki−Miyaura cross-coupling reactions.[65] Ribeiro et al. compared the binding of Cd and Pb to Lewis base sites located on vanillin derivatives. In their case, they found that Pb^{2+} ions had greater molar binding affinities for the Lewis base sites than Cd^{2+} in line with their experimental observations.[66] This led us to employ a comparatively large 40T (144 atoms in total) model of the zeolite A surface to model metal binding.[65,67] The 8T ring is the largest present, and a Lewis base site contained within is the most common metal binding site in such materials.[68−70]

Table 5. Thermodynamic Parameters for the Adsorption of Cd^{2+} and Pb^{2+} on Zeolite A

			$\Delta G°$ (kJ mol^{-1})			
	$\Delta H°$ (kJ mol^{-1})	$\Delta S°$ (J mol^{-1}K^{-1})	293 K	303 K	313 K	323 K
Cd^{2+}	32.11	156.30	−45.76	−47.33	−48.89	−50.45
Pb^{2+}	34.12	139.02	−40.70	−42.09	−43.48	−44.87

https://doi.org/10.1021/acsomega.4c09990
ACS Omega 2025, 10, 5981−5992

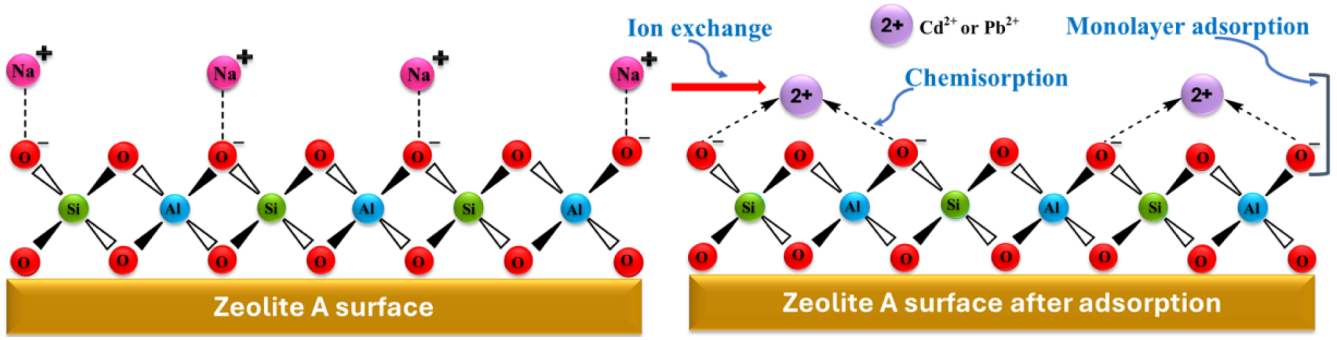

Figure 8. Possible mechanism of Cd^{2+} and Pb^{2+} adsorption on zeolite A.

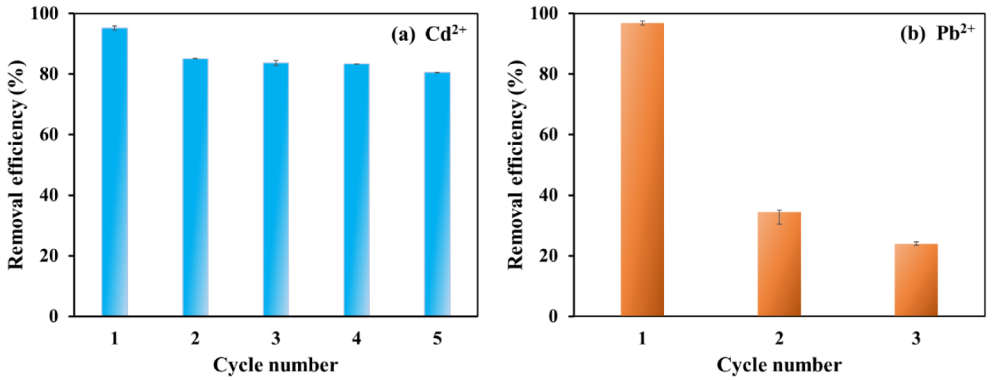

Figure 9. Reusability of zeolite A for Cd^{2+} (a) and Pb^{2+} (b) adsorption.

We assessed the binding of Cd^{2+} and Pb^{2+} ions to zeolite A with a view to understanding why the former shows increased affinity compared to the latter. To this end, we coordinated the ions within the central pore of zeolite A, each forming a bidentate interaction with 2 oxygen atoms on either side of an Al inserted into the pore.[71] Al is a common additive in zeolites and helps increase the Lewis acidity/basicity of the material and imbue it with novel chemical properties.[72,73]

Ions were initially optimized with zeolite A alone, followed by reoptimization in the presence of an increasing number of coordinating water molecules (Figure 10).[74,75] Calculations of the aqueous environment were undertaken, with the ions directly coordinated to increasing numbers of water molecules.

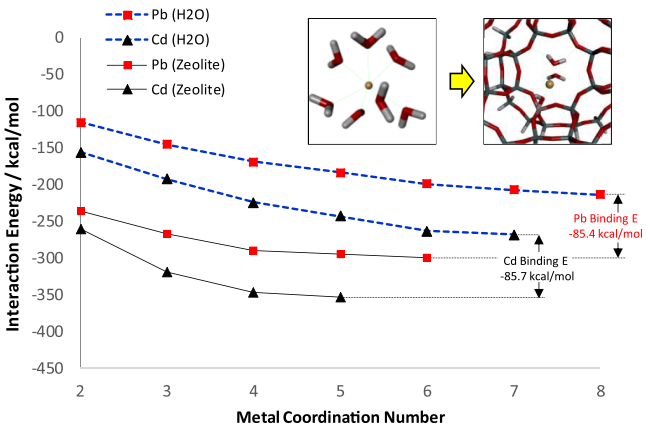

Figure 10. Interaction energies between metal ions and zeolite A or the aqueous solvent model.

Only a single coordination sphere was considered for reasons of computational efficiency.

It can be noted from Figure 10 that, understandably, the metal ions have an increased coordination number in aqueous solution compared to zeolite A. It is also clear that as the coordination number increases, the interaction energy decreases up until the first solvation shell is completed. Pb^{2+} has a greater surface area and can coordinate up to 8 water molecules in its primary coordination sphere. This compares to 7 for the smaller Cd^{2+}. It must be noted that the experimental hydration sphere for Cd^{2+} is larger than Pb^{2+} (Table 6) due to additional water layers.[76]

Table 6. Comparison between Experimental Adsorption Capacities vs Theoretical Data of Binding Energies

		Adsorption Capacities		Theoretical Calculation
Metals	Molar Mass, g/mol	mg/g	μmol/g	Binding Energy, kcal/mol
Cd^{2+}	112	6.50	57.9	−85.72
Pb^{2+}	207	7.90	38.1	−85.39

Turning to zeolite A, we find that the restricted size of the cavity means that the ions have a smaller coordination number, decreasing by 2 for Cd^{2+} and 1 for Pb^{2+}. This suggests that ion binding to the zeolite will result in a favorable entropic effect due to the release of 4−5 water molecules, consistent with what is observed experimentally. The computed binding energy, taken as the difference between the maximum interaction in zeolite A vs solution, points to an exothermic process. However, our experimental thermodynamic data points to an endothermic process. This appears to be a function of (a) the single solvation sphere used for the solution model and (b) the fact that most ions likely bind to weaker Si−O Lewis base sites than our Al-

https://doi.org/10.1021/acsomega.4c09990
ACS Omega 2025, 10, 5981−5992

doped model since impurities within the material are generally relatively low. Nevertheless, the ion binding energies can be assessed in a relative sense to compare the Pb^{2+} and Cd^{2+} ions. Indeed, we find that Cd^{2+} ions show marginally greater affinity for zeolite A compared to Pb^{2+} (−85.72 vs −85.39 kcal/mol), in agreement with the experimental results.

Our simulations show that Cd^{2+} and Pb^{2+} can bind within the 8T cavity located within and on the surface of zeolite A at a Lewis-based site. Due to the relatively small cavity of zeolite A,[77] we predict that the large Pb^{2+} ion is less effectively solvated within the cavity, and this would explain the lower molar binding affinities for the metal compared to Cd^{2+} reported here. Other reports show that DFT methods have also reproduced the experimental binding of Pb^{2+} and Cd^{2+} metals to Lewis acids[66] and show such calculations could potentially be used to aid in the selection of differing zeolites, with differing pore geometries, to selectively trap different metal ions.[78]

3. CONCLUSION

In this study, zeolite A was successfully synthesized from lignite coal fly ash using a hydrothermal method. Various characterization techniques, including XRD, XRF, BET, and SEM, confirmed that the synthesized zeolite closely matched theoretical zeolite A. The potential of zeolite A for removing Cd^{2+} and Pb^{2+} from prepared solutions was further evaluated. The removal efficiencies of zeolite A were high, achieving 99.65% ± 0.1% for Cd^{2+} and 93.90% ± 0.5% for Pb^{2+}. Moreover, zeolite A demonstrated reusability for the adsorption of Cd^{2+} and Pb^{2+}. Isotherm, kinetic, and thermodynamic studies, combined with DFT calculations, were used to investigate the adsorption mechanisms of Cd^{2+} and Pb^{2+} on zeolite A. The results indicated that the adsorption of Cd^{2+} and Pb^{2+} by zeolite A fit the Langmuir isotherm model and the pseudo-second-order kinetic model. Additionally, these adsorption processes were spontaneous and endothermic, as evidenced by increasingly negative values of the Gibbs free energy change (ΔG°) with rising temperature. Therefore, zeolite A synthesized from industrial waste has potential as an adsorbent for the removal of heavy metal ions in real wastewater applications. In the future, we aim to optimize the adsorption performance of zeolite A for real wastewater samples from various industries. Moreover, our research will focus on refining the synthesis process to minimize energy consumption, facilitating the large-scale production of zeolite A from industrial waste. These efforts will contribute to sustainability and support the practical application of zeolite A in real wastewater treatment.

4. MATERIALS AND METHODS

4.1. Materials. Analytical reagent grade chemicals were used in the current work: $NaAlO_2$ (anhydrous, Al (Al_2O_3): 50−56%, Na (as Na_2O): 37−45%, Sigma-Aldrich, USA), NaOH (Carlo Erba Reagents, France, ≥97.0%), HCl (Sd Fine-Chem Limited, India, ≥36.0−38.0% w/w), $Cd(NO_3)_2{\cdot}4H_2O$ (PanReac AppliChem ITW Reagents, USA, ≥99.0%), and $Pb(NO_3)_2$ (Carlo Erba Reagents, France, ≥99.8%). Deionized water was prepared using a water deionizer (WaterPro PS, Labconco, USA).

4.2. Synthesis of Zeolite A. Fly ash obtained from the Mae Moh power plant in Lampang, Thailand, was used for silica extraction. A mixture of fly ash (40 g) and 3 M NaOH at a ratio of 1:10 g/mL was refluxed at 90 °C for 24 h, yielding an Na_2SiO_3 solution. This solution was then filtered using Whatman No.1 filter paper. The filtered Na_2SiO_3 solution was mixed with 3 M HCl and incubated at room temperature for 18 h, producing a silica (SiO_2) precipitate. This precipitate was washed with distilled water until the pH was neutralized to 7, then dried at 80 °C for 18 h, yielding silica powder.

A 5.3 g portion of silica powder in the NaOH solution (10.1 g of NaOH and 71.7 g of water) was heated in a water bath at 100 °C for 45 min, yielding a clear solution. This solution was cooled to room temperature and slowly mixed with a sodium aluminate solution, prepared by dissolving 5.3 g of $NaAlO_2$, 0.3 g of NaOH, and 76.6 g of distilled water, with continuous stirring for 10 min. The obtained mixture was then placed in an oven at 90 °C for 16 h to allow for the crystallization of zeolite A. Zeolite A was filtered, washed with distilled water until the pH was neutralized to 7, and then dried in an oven at 90 °C overnight.[39,40]

4.3. Characterization. The chemical composition of fly ash, silica, and zeolite A was analyzed using a WD-X-ray fluorescence spectrometer (XRF) (ZSX PrimusII, Rigaku, USA). The phase and crystal structure of zeolite A were determined by X-ray diffraction (XRD) (X'Pert Pro, PANalytical, Netherlands) with Cu Kα radiation (λ = 1.5406 Å) at 40 kV and 30 mA. The surface area and particle size distribution of zeolite A were measured by Brunauer−Emmett−Teller (BET) (ASAP2460, Micromeritics, USA). The morphology of zeolite A was examined by using a scanning electron microscope (SEM) (SSX-550, Shimadzu, Japan).

4.4. Study on Adsorbent Dosage. Zeolite A dosages were varied from 0.025 g, 0.05 g, 0.10 g, 0.15 g, and 0.20 g, to 0.25 g for Cd^{2+} adsorption, and from 0.025 g, 0.05 g, 0.10 g, and 0.15 g, to 0.20 g for Pb^{2+} adsorption. The adsorption of Cd^{2+} and Pb^{2+} by different dosages of zeolite A was investigated through a batch experiment using 25 mL of Cd^{2+} and Pb^{2+} solutions with an initial concentration of 50 mg/L, prepared by diluting a 1000 mg/L stock solution of $Cd(NO_3)_2{\cdot}4H_2O$ and $Pb(NO_3)_2$. This resulted in zeolite A concentrations of 1 g/L, 2 g/L, 4 g/L, 6 g/L, 8 g/L, and 10 g/L for Cd^{2+} adsorption, and 1 g/L, 2 g/L, 4 g/L, 6 g/L, and 8 g/L for Pb^{2+} adsorption in each 25 mL batch. A contact time of 60 min at 25 °C was maintained for each adsorption batch. Subsequently, zeolite A was separated using a paper filter, and the filtrate was collected for analysis of the residual concentrations of Cd^{2+} and Pb^{2+} using an atomic absorption spectrophotometer (AAS) (AAnalyst 800, PerkinElmer, USA). The removal efficiency (R%) and adsorption capacity (q) of Cd^{2+} and Pb^{2+} by each dosage of zeolite A were calculated using eqs 1 and 2, respectively. The zeolite A dosage that exhibited the highest adsorption capacity was selected as the optimal dosage for the further investigation of Cd^{2+} and Pb^{2+} adsorption.

$$R\% = \frac{C_0 - C_e}{C_0} \times 100\% \quad (1)$$

$$q = \frac{C_0 - C_e}{m} \times V \quad (2)$$

C_0 and C_e represent the initial and residual concentrations (mg/L) of Cd^{2+} and Pb^{2+}, respectively. V denotes the volume (L) of each adsorption bath, and m refers to the mass (g) of zeolite A.

4.5. Study on Contact Time and Adsorption Kinetics. The optimal dosages of zeolite A for Cd^{2+} and Pb^{2+} adsorption were used to evaluate the effect of different contact times: 15, 30, 60, 120, 240, and 720 min on the adsorption of Cd^{2+} and Pb^{2+}. The batch experiment for adsorption and the analysis of the residual concentrations of Cd^{2+} and Pb^{2+} are described above.

https://doi.org/10.1021/acsomega.4c09990
ACS Omega 2025, 10, 5981−5992

The removal efficiency was calculated for each contact time. The shortest contact time that achieved the highest removal efficiency was selected as the optimal contact time for the adsorption isotherm study of Cd^{2+} and Pb^{2+}.

The results from the study of the effect of contact time on the adsorption of Cd^{2+} and Pb^{2+} by zeolite A were further used for kinetic studies using the pseudo-first-order model and the pseudo-second-order model,[41,42] as described by eqs 3 and 4, respectively.

$$\ln(q_e - q_t) = -k_1 t + \ln q_e \tag{3}$$

$$\frac{t}{q_t} = \left(\frac{1}{q_e}\right)t + \frac{1}{k_2 q_e^2} \tag{4}$$

q_e and q_t represent the adsorption capacity at equilibrium and the adsorption capacity at each contact time (t), respectively. k_1 and k_2 are the rate constants for the pseudo-first-order and pseudo-second-order models, respectively.

4.6. Study on Adsorption Isotherms. The initial concentrations of Cd^{2+} and Pb^{2+} at 50, 100, 150, 200, and 250 mg/L were used for the adsorption isotherm study. The adsorption of Cd^{2+} and Pb^{2+} at these different initial concentrations was investigated through a batch experiment using 25 mL of Cd^{2+} and Pb^{2+} solutions, the optimal dosage of zeolite A, and the optimal contact time at 25 °C. Subsequently, zeolite A was separated using a paper filter, and the filtrate was collected for the analysis of the residual concentrations of Cd^{2+} and Pb^{2+} using an atomic absorption spectrophotometer. The removal efficiency and adsorption capacity of Cd^{2+} and Pb^{2+} for each initial concentration were then calculated by using eqs 1 and 2, respectively. The Langmuir and Freundlich models,[43,44] expressed by eqs 5 and 7 respectively, were used to investigate the adsorption isotherms of Cd^{2+} and Pb^{2+} onto zeolite A.

$$\frac{C_e}{q} = \left(\frac{1}{q_{max}}\right)C_e + \frac{1}{K_L q_{max}} \tag{5}$$

$$R_L = \frac{1}{1 + K_L C_0} \tag{6}$$

q and C_e represent the adsorption capacity (mg/g) and residual concentration (mg/L) of Cd^{2+} and Pb^{2+} for each initial concentration, respectively. The plot of $\frac{C_e}{q}$ versus C_e resulted in a linear line with a slope and intercept equal to $\frac{1}{q_{max}}$ and $\frac{1}{K_L q_{max}}$, respectively. Here, q_{max} is the maximum adsorption capacity (mg/g) of Cd^{2+} or Pb^{2+} on zeolite A, and K_L is the Langmuir constant (L/mg). Thus, q_{max} for the adsorption of Cd^{2+} or Pb^{2+} by zeolite A and K_L were calculated as $\frac{1}{\text{slope}}$ and $\frac{1}{\text{intercept} \times q_{max}}$, respectively. Moreover, the equilibrium parameter (R_L) values,[45] which indicate the favorability of adsorption of Cd^{2+} or Pb^{2+} by zeolite A, were calculated from K_L and C_0 values as described by eq 6. $R_L > 1$, $R_L < 1$, and $R_L = 0$ indicate unfavorable, favorable, and irreversible adsorption, respectively. In this work, R_L values were calculated for each initial concentration of Cd^{2+} and Pb^{2+} and are reported as an interval of R_L values.

$$\log q = \left(\frac{1}{n}\right)\log C_e + \log K_F \tag{7}$$

The plot of log q versus log C_e from the Freundlich equation (eq 7) resulted in a linear line with a slope and intercept corresponding to $\frac{1}{n}$ and log K_F, respectively. K_F and n are the Freundlich constant and heterogeneity factor, respectively.

4.7. Study of Thermodynamics. The adsorption experiments of Cd^{2+} and Pb^{2+} by zeolite A were conducted at different temperatures (293, 303, 313, and 323 K) using the optimal dosage, optimal contact time of zeolite A, and 25 mL of 50 mg/L Cd^{2+} and Pb^{2+} solutions as the initial concentration for the thermodynamic study. The residual concentrations of Cd^{2+} and Pb^{2+} in the solution after the adsorption experiment at each temperature were analyzed by using an atomic absorption spectrophotometer. Gibbs free energy change (ΔG°) was calculated using eqs 8 and 9. The combination of these two equations resulted in eq 10. The entropy change (ΔS°) and enthalpy change (ΔH°) for the adsorption process were determined from the linear plot of ln K_d versus $\frac{1}{T}$, where K_d is the equilibrium constant calculated using eq 11, and T is the temperature of the adsorption experiment. ΔS° and ΔH° were calculated from the slope ($\frac{\Delta H^\circ}{R}$) and intercept ($\frac{\Delta S^\circ}{R}$) of this plot, respectively. The calculated ΔS° and ΔH° values were then used to determine the ΔG° value (using eq 9) for the adsorption of Cd^{2+} or Pb^{2+} by zeolite A at each temperature.[46]

$$\Delta G^\circ = -RT\ln K_d \tag{8}$$

$$\Delta G^\circ = \Delta H^\circ - T\Delta S^\circ \tag{9}$$

$$\ln K_d = -\frac{\Delta H^\circ}{R}\left(\frac{1}{T}\right) + \frac{\Delta S^\circ}{R} \tag{10}$$

$$K_d = \frac{q_t}{C_t} \tag{11}$$

q_t (mg/g) and C_t (mg/L) represent the adsorption capacity and the residual concentration of Cd^{2+} and Pb^{2+} at each temperature, respectively. R is the gas constant (8.314 J mol^{-1} K^{-1}).

4.8. Study of Reusability of Zeolite A. The reusability of zeolite A for removing Cd^{2+} and Pb^{2+} was investigated through batch experiments using the optimal dosage of zeolite A, optimal contact time, and 25 mL of 50 mg/L Cd^{2+} and Pb^{2+} solutions as the initial concentration at 25 °C. Zeolite A was then separated using a paper filter, and the filtrate was collected for analysis of the residual concentrations of Cd^{2+} and Pb^{2+} using an atomic absorption spectrophotometer. The separated zeolite was dried in an oven at 90 °C overnight. 0.1 g of the dried zeolite A sample was washed with 100 mL of 1 M NaCl at a stirring speed of 250 rpm for 10 h at 25 °C to desorb Cd^{2+} and Pb^{2+}.[47] Zeolite A was then collected and dried in an oven at 90 °C overnight to obtain regenerated zeolite A, which was used to assess the reusability of the adsorbent. The regenerated zeolite A was divided into three portions of the optimal dosage for three duplicates of reuse cycles of Cd^{2+} and Pb^{2+} adsorption. The removal efficiency of zeolite A for each cycle was calculated using eq 1. The reuse cycles of Cd^{2+} and Pb^{2+} adsorption by the regenerated zeolite A were repeated until the removal efficiency significantly decreased.

4.9. Computational Studies. A 40T cluster model of Zeolite A (Linde Type A, LTA) was adapted from the crystal structure reported in the zeolite structure database (http://www.izastructure.org/databases). A single Si atom was replaced with an Al atom in the 8-membered ring.[48] The dangling bonds

https://doi.org/10.1021/acsomega.4c09990
ACS Omega 2025, 10, 5981−5992

of the terminal silicon or oxygen atoms of the 40T model were terminated with H atoms and fixed to maintain the zeolite framework in the correct 3D structure during optimization. The adsorption of Pb^{2+} and Cd^{2+} to the zeolite was investigated using DFT with the M06 functional implemented in the Gaussian 16 package.[49] Si, O, and H atoms were treated using the 6-31G* basis set, and QZVP was used to describe Pb^{2+} and Cd^{2+} metals. Models of Pb^{2+} and Cd^{2+} coordinated with water were also evaluated. The relative affinity of the ions for the zeolite versus water phases was calculated as the difference between the interaction in the zeolite model minus the value from the water model.

■ ASSOCIATED CONTENT

Supporting Information

The Supporting Information is available free of charge at https://pubs.acs.org/doi/10.1021/acsomega.4c09990.

Further details of characterization results, namely X-ray fluorescence (XRF), X-ray diffraction (XRD), and thermogravimetric analysis (TGA) techniques (PDF)

■ AUTHOR INFORMATION

Corresponding Author

Pornpan Pungpo − *Department of Chemistry and Center of Excellence for Innovation in Chemistry, Faculty of Science, Ubon Ratchathani University, Ubon Ratchathani 34190, Thailand;* orcid.org/0000-0001-6278-7943; Email: pornpan_ubu@yahoo.com

Authors

Darunee Sukchit − *Department of Chemistry and Center of Excellence for Innovation in Chemistry, Faculty of Science, Ubon Ratchathani University, Ubon Ratchathani 34190, Thailand;* orcid.org/0000-0002-5374-4711

Malee Prajuabsuk − *Department of Chemistry and Center of Excellence for Innovation in Chemistry, Faculty of Science, Ubon Ratchathani University, Ubon Ratchathani 34190, Thailand*

Saisamorn Lumlong − *Department of Chemistry and Center of Excellence for Innovation in Chemistry, Faculty of Science, Ubon Ratchathani University, Ubon Ratchathani 34190, Thailand*

Chan Inntam − *Department of Chemistry and Center of Excellence for Innovation in Chemistry, Faculty of Science, Ubon Ratchathani University, Ubon Ratchathani 34190, Thailand*

Auradee Punkvang − *Division of Chemistry, Faculty of Science, Nakhon Phanom University, Nakhon Phanom 48000, Thailand;* orcid.org/0000-0002-0325-9179

Sasijuta Wattanarach − *National Metal and Materials Technology Center, National Science and Technology Development Agency (NSTDA), Pathum Thani 12120, Thailand*

Parjaree Thavorniti − *National Metal and Materials Technology Center, National Science and Technology Development Agency (NSTDA), Pathum Thani 12120, Thailand*

Bunjerd Jongsomjit − *Center of Excellence on Catalysis and Catalytic Reaction Engineering, Department of Chemical Engineering, Faculty of Engineering, Chulalongkorn University, Bangkok 10330, Thailand; Bio-Circular-Green-Economy Technology & Engineering Center, BCGeTEC, Department of Chemical Engineering, Faculty of Engineering, Chulalongkorn University, Bangkok 10330, Thailand;* orcid.org/0000-0002-9558-9190

Kanitta Wongyai − *Laboratory Section, Geology Department, Mae Moh Mine, Electricity Generating Authority of Thailand (EGAT), Lampang 52220, Thailand*

Duangkamol Gleeson − *Applied Computational Chemistry Research Unit and Department of Chemistry, School of Science, King Mongkut's Institute of Technology Ladkrabang, Bangkok 10520, Thailand;* orcid.org/0000-0001-5845-6842

Paramasivam Shanmugam − *Department of Chemistry, Faculty of Science and Technology, Thammasat University, Pathum Thani 12120, Thailand;* orcid.org/0000-0002-9535-8771

Supakorn Boonyuen − *Department of Chemistry, Faculty of Science and Technology, Thammasat University, Pathum Thani 12120, Thailand*

Complete contact information is available at: https://pubs.acs.org/10.1021/acsomega.4c09990

Author Contributions

D.S., S.W., and P.S. performed the investigations. D.S. wrote the original draft of the manuscript. M.P., S.L., C.I., A.P., P.T., B.J., K.W., P.S., S.B., and D.G. revised and edited the manuscript. P.P. performed funding acquisition, conceptualization, review, editing, and project administration.

Notes

The authors declare no competing financial interest.

■ ACKNOWLEDGMENTS

This research was supported by Ubon Ratchathani University. The research on the "Synthesis and characterization of zeolite A from industrial fly ash as a green, cost-effective Cd^{2+} and Pb^{2+} adsorbent for wastewater applications" by Ubon Ratchathani University, Department of Chemistry, has received funding support from the NSRF. We would like to thank Mae Moh Power Plant, Lampang Province, for providing fly ash in this study. The Thailand Graduate Institute of Science and Technology (SCA-CO-2565-17147-TH) is acknowledged for financial support to D. Sukchit. Ubon Ratchathani University, National Metal and Materials Technology Center, and National Science and Technology Development Agency (NSTDA) are gratefully acknowledged for supporting this research.

■ REFERENCES

(1) Amran, M.; Fediuk, R.; Murali, G.; Avudaiappan, S.; Ozbakkaloglu, T.; Vatin, N.; Karelina, M.; Klyuev, S.; Gholampour, A. Fly Ash-Based Eco-Efficient Concretes: A Comprehensive Review of the Short-Term Properties. *Materials* **2021**, *14*, 4264.

(2) ASTM International. *Standard Specification for Coal Fly Ash and Raw or Calcined Natural Pozzolan for Use in Concrete*. ASTM International: 2017.

(3) Cho, H.; Oh, D.; Kim, K. A study on removal characteristics of heavy metals from aqueous solution by fly ash. *J. Hazard. Mater.* **2005**, *127*, 187−195.

(4) Yao, Z. T.; Ji, X. S.; Sarker, P. K.; Tang, J. H.; Ge, L. Q.; Xia, M. S.; Xi, Y. Q. A comprehensive review on the applications of coal fly ash. *Earth-Sci. Rev.* **2015**, *141*, 105−121.

(5) Murukutti, M. K.; Jena, H. Synthesis of nano-crystalline zeolite-A and zeolite-X from Indian coal fly ash, its characterization and performance evaluation for the removal of Cs^{+} and Sr^{2+} from simulated nuclear waste. *J. Hazard. Mater.* **2022**, *423*, 127085.

(6) Xing, L.; Li, X.; Cao, P.; Luo, J.; Jiang, H. Stepwise extraction and utilization of silica and alumina from coal fly ash by mild hydrothermal process. *Process Saf. Environ. Prot.* **2024**, *182*, 918−929.
(7) Khaleque, A.; Alam, M. M.; Hoque, M.; Mondal, S.; Haider, J. B.; Xu, B.; Johir, M. A. H.; Karmakar, A. K.; Zhou, J. L.; Ahmed, M. B.; et al. Zeolite synthesis from low-cost materials and environmental applications: A review. *Environ. Adv.* **2020**, *2*, 100019.
(8) Hu, G.; Yang, J.; Duan, X.; Farnood, R.; Yang, C.; Yang, J.; Liu, W.; Liu, Q. Recent developments and challenges in zeolite-based composite photocatalysts for environmental applications. *Chem. Eng. J.* **2021**, *417*, 129209.
(9) Szerement, J.; Szatanik-Kloc, A.; Jarosz, R.; Bajda, T.; Mierzwa-Hersztek, M. Contemporary applications of natural and synthetic zeolites from fly ash in agriculture and environmental protection. *Chem. Eng. J.* **2021**, *311*, 127461.
(10) Algieri, C.; Drioli, E. Zeolite membranes: Synthesis and applications. *Sep. Purif. Technol.* **2021**, *278*, 119295.
(11) Yue, B.; Liu, S.; Chai, Y.; Wu, G.; Guan, N.; Li, L. Zeolites for separation: Fundamental and application. *J. Energy Chem.* **2022**, *71*, 288−303.
(12) Serati-Nouri, H.; Jafari, A.; Roshangar, L.; Dadashpour, M.; Pilehvar-Soltanahmadi, Y.; Zarghami, N. Biomedical applications of zeolite-based materials: A review. *Mater. Sci. Eng., C* **2020**, *116*, 111225.
(13) Farghali, M. A.; Abo-Aly, M. M.; Salaheldin, T. A. Modified mesoporous zeolite-A/reduced graphene oxide nanocomposite for dual removal of methylene blue and Pb^{2+} ions from wastewater. *Inorg. Chem. Commun.* **2021**, *126*, 108487.
(14) Obaid, S. S.; Gaikwad, D. K.; Sayyed, M. I.; Khader, A. R.; Pawar, P. P. Heavy metal ions removal from waste water bythe natural zeolites. *Mater. Today: Proc.* **2018**, *5*, 17930−17934.
(15) Wang, S.; Peng, Y. Natural zeolites as effective adsorbents in water and wastewater treatment. *Chem. Eng. J.* **2010**, *156*, 11−24.
(16) Hong, M.; Yu, L.; Wang, Y.; Zhang, J.; Chen, Z.; Dong, L.; Zan, Q.; Li, R. Heavy Metal Adsorption with Zeolites: The Role of Hierarchical Pore Architecture. *Chem. Eng. J.* **2019**, *359*, 363−372.
(17) Sathupunya, M.; Gulari, E.; Wongkasemjit, S. Na-A (LTA) zeolite synthesis directly from alumatrane and silatrane by sol-gel microwave techniques. *J. Eur. Ceram. Soc.* **2003**, *23*, 1293−1303.
(18) Meng, Q.; Chen, H.; Lin, J.; Lin, Z.; Sun, J. Zeolite A synthesized from alkaline assisted pre-activated halloysite for efficient heavy metal removal in polluted river water and industrial wastewater. *J. Environ. Sci* **2017**, *56*, 254−262.
(19) Bao, W.; Liu, L.; Zou, H.; Gan, S.; Xu, X.; Ji, G.; Gao, G.; Zheng, K. Removal of Cu^{2+} from Aqueous Solutions Using Na-A Zeolite from Oil Shale Ash. *Chin. J. Chem. Eng.* **2013**, *21*, 974−982.
(20) Zayed, A. M.; Selim, A. Q.; Mohamed, E. A.; Wahed, M. S. A.; Seliem, M. K.; Sillanpää, M. Adsorption characteristics of Na-A zeolites synthesized from Egyptian kaolinite for manganese in aqueous solutions: Response surface modeling and optimization. *Appl. Clay Sci.* **2017**, *140*, 17−24.
(21) Nadeem, S.; Mutalib, I. A.; Shahrun, M. S. Synthesis of metalloporphyrin encapsulated zeolite A for photocatalytic orange II degradation. *Procedia Eng* **2016**, *148*, 1282−1288.
(22) Panayotova, M.; Velikov, B. Kinetics of heavy metal ions removal by use of natural zeolite. *J. Environ. Sci. Health* **2002**, *37*, 139−147.
(23) Chen, Y.; Zhao, W.; Wang, H.; Meng, X.; Zhang, L. A novel polyamine-type starch/glycidyl methacrylate copolymer for adsorption of Pb(II), Cu(II), Cd(II) and Cr(III) ions from aqueous solutions. *R. Soc. Open Sci.* **2018**, *5*, 180281.
(24) Barakat, M. A. New trends in removing heavy metals from industrial wastewater. *Arab. J. Chem.* **2011**, *4*, 361−377.
(25) Tchounwou, P. B.; Yedjou, C. G.; Patlolla, A. K.; Sutton, D. J. Heavy Metals Toxicity and the Environment. *Molecular, Clinical and Environmental Toxicology*; Springer Science & Business Media, 2012; Vol. *101*, pp 133−164.
(26) Mahmoud, A. E. D.; Mostafa, E. Nanofiltration Membranes for the Removal of Heavy Metals from Aqueous Solutions: Preparations and Applications. *Membranes* **2023**, *13*, 789.
(27) Vital, B.; Bartacek, J.; Ortega-Bravo, J. C.; Jeison, D. Treatment of acid mine drainage by forward osmosis: Heavy metal rejection and reverse flux of draw solution constituents. *Chem. Eng. J.* **2018**, *332*, 85−91.
(28) Xiang, H.; Min, X.; Tang, C.J.; Sillanpää, M.; Zhao, F. Recent advances in membrane filtration for heavy metal removal from wastewater: A mini review. *J. Water Process. Eng.* **2022**, *49*, 103023.
(29) Zhang, Y.; Feng, Y.; Xiang, Q.; Liu, F.; Ling, C.; Wang, F.; Li, Y.; Li, A. A high-flux and anti-interference dual-functional membrane for effective removal of Pb(II) from natural water. *J. Hazard. Mater.* **2020**, *384*, 121492.
(30) Rasaki, S. A.; Thomas, T.; Yang, M. Co-precipitation strategy for engineering pH tolerant and durable ZnO@MgO nanospheres for efficient, room-temperature, chemisorptive removal of Pb(II) from water. *J. Environ. Chem. Eng.* **2019**, *7*, 103019.
(31) Yan, J.; Yuan, W.; Liu, J.; Ye, W.; Lin, J.; Xie, J.; Huang, X.; Gao, S.; Xie, J.; Liu, S.; Chen, W.; Zhang, H. An integrated process of chemical precipitation and sulfate reduction for treatment of flue gas desulphurization wastewater from coal fired power plant. *J. Cleaner Prod.* **2019**, *228*, 63−72.
(32) Munoz-Morales, M.; Saez, C.; Cañizares, P.; Rodrigo, M. A. A new strategy for the electrolytic removal of organics based on adsorption onto granular activated carbon. *Electrochem. Commun.* **2018**, *90*, 47−50.
(33) Bezzina, J. P.; Ruder, L. R.; Dawson, R.; Ogden, M. D. Ion exchange removal of Cu (II), Fe(II), Pb(II) and Zn(II) from acid extracted sewage sludge - Resin screening in weak acid media. *Water Res.* **2019**, *158*, 257−267.
(34) Zhang, Q.; Pan, B.; Zhang, W.; Pan, B.; Lv, L.; Wang, X.; Wu, J.; Tao, X. Selective removal of Pb(II), Cd(II), and Zn(II) ions from waters by an inorganic exchanger Zr $(HPO_3S)_2$. *J. Hazard. Mater.* **2009**, *170*, 824−828.
(35) Yu, W.; Yuan, P.; Liu, D.; Deng, L.; Yuan, W.; Tao, B.; Cheng, H.; Chen, F. Facile preparation of hierarchically porous diatomite/MFI-type zeolite composites and their performance of benzene adsorption: The effects of NaOH etching pretreatment. *J. Hazard. Mater.* **2015**, *285*, 173−181.
(36) Alqadami, A. A.; Naushad, M.; ALOthman, Z. A.; Alsuhybani, M.; Algamdi, M. Excellent adsorptive performance of a new nanocomposite for removal of toxic Pb(II) from aqueous environment: Adsorption mechanism and modeling analysis. *J. Hazard. Mater.* **2020**, *389*, 121896.
(37) Kazak, O.; Tor, A. In situ preparation of magnetic hydrochar by co-hydrothermal treatment of waste vinasse with red mud and its adsorption property for Pb(II) in aqueous solution. *J. Hazard. Mater.* **2020**, *393*, 122391.
(38) Qu, J.; Tian, X.; Jiang, Z.; Cao, B.; Akindolie, M. S.; Hu, Q.; Feng, C.; Feng, Y.; Meng, X.; Zhang, Y. Multi-component adsorption of Pb(II), Cd(II) and Ni(II) onto microwave-functionalized cellulose: Kinetics, isotherms, thermodynamics, mechanisms and application for electroplating wastewater purification. *J. Hazard. Mater.* **2020**, *387*, 121718.
(39) Azizi, S. N.; Dehnavi, A. R.; Joorabdoozha, A. Synthesis and characterization of LTA nanozeolite using barley husk silica: Mercury removal from standard and real solutions. *Mater. Res. Bull.* **2013**, *48*, 1753−1759.
(40) Tohdee, K.; Semmad, S.; Nonthawong, J.; Praserthdam, P.; Pungpo, P.; Jongsomjit, B. Characteristics and catalytic properties of WO_3 supported on zeolite A-derived from fly ash of sugarcane bagasse via esterification of ethanol and lactic acid. *S. Afr. J. Chem. Eng.* **2024**, *49*, 273−284.
(41) Lagergren, S.*About the theory of so-called adsorption of soluble substances*Kungliga Svenska Vetenskapsakademiens Handlingar1898241−39
(42) Ho, Y. S.; McKay, G. Pseudo-second order model for sorption processes. *Process Biochem.* **1999**, *34*, 451−465.
(43) Langmuir, I. The constitution and fundamental properties of solids and liquids, Part 1, solids. *J. Am. Chem. Soc.* **1916**, *38*, 2221−2295.

https://doi.org/10.1021/acsomega.4c09990
ACS Omega 2025, 10, 5981−5992

(44) Freundlich, H. M. F. Over the adsorption in solution. *Z. Phys. Chem.* **1906**, *57*, 385−470.
(45) Hall, K. R.; Eagleton, L. C.; Acrivos, A.; Vermeulen, T. Pore- and solid-diffusion kinetics in fixed-bed adsorption under constant-pattern conditions. *Ind. Eng. Chem. Fundam.* **1966**, *5*, 212−223.
(46) Laidler, K. J.; Meiser, J. H. *Physical Chemistry*; Houghton Mifflin: New York, 1999; p 852.
(47) Su, Q.; He, Y.; Yang, S.; Wan, H.; Chang, S.; Cui, X. Synthesis of NaA-zeolite microspheres by conversion of geopolymer and their performance of Pb (II) removal. *Appl. Clay Sci.* **2021**, *200*, 105914.
(48) Liu, Y.; Yang, D.; Shang, J.; Zhou, J.; Chang, V. Direct decomposition of NO over 8MR in high silica Cu-LTA zeolite: A DFT study on reaction mechanisms, thermodynamics and kinetics. *Mol. Catal.* **2022**, *530*, 112602.
(49) Frisch, M. J.; Trucks, G. W.; Schlegel, H. B.; Scuseria, G. E.; Robb, M. A.; Cheeseman, J. R.; Scalmani, G.; Barone, V.; Petersson, G. A.; Nakatsuji, H.; *Gaussian 16, Revision B.01*, Gaussian, Inc., Wallingford CT, 2016.
(50) Jayaranjan, M. L. D.; Van Hullebusch, E. D.; Annachhatre, A. P. Reuse options for coal fired power plant bottom ash and fly ash. *Rev. Environ. Sci. Biotechnol.* **2014**, *13*, 467−486.
(51) Lee, Y.-R.; Soe, J. T.; Zhang, S.; Ahn, J.-W.; Park, M. B.; Ahn, W.-S. Synthesis of nanoporous materials via recycling coal fly ash and other solid wastes: A mini review. *Chem. Eng. J* **2017**, *317*, 821−843.
(52) Ma, G.; Bai, C.; Wang, M.; He, P. Effects of Si/Al Ratios on the Bulk-Type Zeolite Formation Using Synthetic Metakaolin-Based Geopolymer with Designated Composition. *Crystals* **2021**, *11*, 1310.
(53) Ji, W.; Feng, N.; Zhao, P.; Zhang, S.; Zhang, S.; Lan, L.; Huang, H.; Li, K.; Sun, Y.; Li, Y; et al. Synthesis of Single-Phase Zeolite A by Coal Gasification Fine Slag from Ningdong and Its Application as a High-Efficiency Adsorbent for Cu^{2+} and Pb^{2+} in Simulated Waste Water. *Chem. Eng. J.* **2020**, *4*, 65.
(54) Kuenzel, C.; Ranjbar, N. Dissolution mechanism of fly ash to quantify the reactive aluminosilicates in geopolymerisation. *Resour., Conserv. Recycl.* **2019**, *150*, 104421.
(55) Maponya, T. C.; Makgopa, K.; Somo, T. R.; Modibane, K. D. Highlighting the Importance of Characterization Techniques Employed in Adsorption Using Metal−Organic Frameworks for Water Treatment. *Polymers* **2022**, *14*, 3613.
(56) Lv, Y.; Ma, B.; Liu, Y.; Wang, C.; Chen, Y. Adsorption behavior and mechanism of mixed heavy metal ions by zeolite adsorbent prepared from lithium leach residue. *Microporous Mesoporous Mater.* **2022**, *329*, 111553.
(57) Malliou, E.; Loizidou, M.; Spyrellis, N. Uptake of lead and cadmium by clinoptilolite. *Sci. Total Environ.* **1994**, *149*, 139−144.
(58) Babel, S.; Kurniawan, T. A. Low-cost adsorbents for heavy metals uptake from contaminated water: A review. *J. Hazard. Mater.* **2003**, *97*, 219−243.
(59) Wanyonyi, F. S.; Orata, F.; Mutua, G. K.; Odey, M. O.; Zamisa, S.; Ogbodo, S. E.; Maingi, F.; Pembere, A. Application of South African heulandite (HEU) zeolite for the adsorption and removal of Pb^{2+} and Cd^{2+} ions from aqueous water solution: Experimental and computational study. *Heliyon* **2024**, *10*, No. e34657.
(60) Chen, M.; Nong, S.; Zhao, Y.; Riaz, M. S.; Xiao, Y.; Molokeev, M. S.; Huang, F. Renewable P-type zeolite for superior absorption of heavy metals: Isotherms, kinetics, and mechanism. *Sci. Total Environ.* **2020**, *726*, 138535.
(61) Fan, X.; Liu, H.; Anang, E.; Ren, D. Effects of electronegativity and hydration energy on the selective adsorption of heavy metal ions by synthetic NaX zeolite. *Mater* **2021**, *14*, 4066.
(62) Rondón, W.; Freire, D.; de Benzo, Z.; Sifontes, A. B.; González, Y.; Valero, M.; Brito, J. L. Application of 3A zeolite prepared from Venezuelan kaolin for removal of Pb (II) from wastewater and Its determination by flame atomic absorption spectrometry. *Am. J. Anal. Chem.* **2013**, *4*, 584−593.
(63) Jangkorn, S.; Youngme, S.; Praipipat, P. Comparative lead adsorptions in synthetic wastewater by synthesized zeolite A of recycled industrial wastes from sugar factory and power plant. *Heliyon* **2022**, *8*, No. e09323.
(64) Liu, Y.; Yan, C.; Zhang, Z.; Wang, H.; Zhou, S.; Zhou, W. A comparative study on fly ash, geopolymer and faujasite block for Pb removal from aqueous solution. *Fuel* **2016**, *185*, 181−189.
(65) Boekfa, B.; Maihom, T.; Ehara, M.; Limtrakul, J. Investigation of the Suzuki−Miyaura cross-coupling reaction on a palladium H-beta zeolite with DFT calculations. *Sci. Rep.* **2024**, *14* (1), 611.
(66) Ribeiro, I. H. S.; Reis, D. T.; Pereira, D. H. A DFT-based analysis of adsorption of Cd^{2+}, Cr^{3+}, Cu^{2+}, Hg^{2+}, Pb^{2+}, and Zn^{2+}, on vanillin monomer: A study of the removal of metal ions from effluents. *J. Mol. Model.* **2019**, *25* (9), 267.
(67) Sittiwong, J.; Prasertsab, A.; Boonmark, S.; Nunthakitgoson, W.; Srifa, P.; Maihom, T.; Limtrakul, J. Theoretical insights into furfural reduction to furfuryl alcohol via the catalytic hydrogen transfer reaction catalyzed by cations exchanged zirconium-containing zeolites. *Mol. Catal.* **2021**, *504*, 111471.
(68) Huang, M.; Kaliaguine, S.; Auroux, A. Lewis basic and Lewis acidic sites in zeolites. *Stud. Surf. Sci. Catal.* **1995**, *97*, 311−318.
(69) Singh, V.; Pant, N.; Sharma, R. K.; Padalia, D.; Rawat, P. S.; Goswami, R.; Singh, P.; Kumar, A.; Bhandari, P.; Tabish, A.; Deifalla, M. A. Adsorption Studies of Pb(II) and Cd(II) Heavy Metal Ions from Aqueous Solutions Using a Magnetic Biochar Composite Material. *Sep* **2023**, *10* (7), 389.
(70) Greń, W.; Parker, S. C.; Slater, B.; Lewis, D. W. Structure of Zeolite A (LTA) Surfaces and the Zeolite A/Water Interface. *J. Phys. Chem. C* **2010**, *114* (21), 9739−9747.
(71) Zhang, J.; Zakeri, T.; Yue, Q.; Kubů, M.; Barakov, R.; Přech, J.; Opanasenko, M.; Shamzhy, M. Lewis acid zeolite catalysts via chemical modification of extra-large pore germanosilicates. *Catal. Today* **2024**, *440*, 114825.
(72) Batool, S. R.; Sushkevich, V. L.; van Bokhoven, J. A. Correlating Lewis acid activity to extra-framework aluminum species in zeolite Y introduced by Ion-exchange. *J. Catal.* **2022**, *408*, 24−35.
(73) Liu, Q.; van Bokhoven, J. A. Water structures on acidic zeolites and their roles in catalysis. *Chem. Soc. Rev.* **2024**, *53*, 3065−3095.
(74) Stanciakova, K.; Ensing, B.; Goltl, F.; Bulo, R. E.; Weckhuysen, B. M. Cooperative Role of Water Molecules during the Initial Stage ofWater-Induced Zeolite Dealumination. *ACS Catal.* **2019**, *9*, 5119−5135.
(75) Jungsuttiwong, S.; Limtrakul, J.; Truong, T. N. Theoretical Study of Modes of Adsorption of Water Dimer on H-ZSM-5 and H-Faujasite Zeolites. *J. Phys. Chem. B* **2005**, *109*, 13342−13351.
(76) Wan, J.; Zhang, F.; Han, Z.; Song, L.; Zhang, C.; Zhang, J. Adsorption of Cd^{2+} and Pb^{2+} by biofuel ash-based geopolymer synthesized by one-step hydrothermal method. *Arab. J. Chem.* **2021**, *14*, 103234.
(77) Danilczuk, M.; Lund, A. Adsorption of NO in Li-exchanged zeolite A. A density functional theory study. *Chem. Phys. Lett.* **2010**, *490*, 205−209.
(78) Wander, M. C. F.; Clark, A. E. Hydration Properties of Aqueous Pb(II) Ion. *Inorg. Chem.* **2008**, *47* (18), 8233−8841.

https://doi.org/10.1021/acsomega.4c09990
ACS Omega 2025, 10, 5981−5992